Bethe-Salpeter calculation of optical-absorption spectra of In_2O_3 and Ga_2O_3

Joel B. Varley[1, *] and André Schleife[2, †]

[1]*Condensed Matter and Materials Division, Lawrence Livermore National Laboratory, Livermore, CA 94550, USA*
[2]*Department of Materials Science and Engineering, University of Illinois at Urbana-Champaign, Urbana, IL 61801, USA*
(Dated: September 25, 2014)

Transparent conducting oxides keep attracting strong scientific interest not only due to their promising potential for "transparent electronics" applications but also due to their intriguing optical absorption characteristics. Materials such as In_2O_3 and Ga_2O_3 have complicated unit cells and, consequently, are interesting systems for studying the physics of excitons and anisotropy of optical absorption. Since currently no experimental data is available, for instance, for their dielectric functions across a large photon-energy range, we employ modern first-principles computational approaches based on many-body perturbation theory to provide theoretical-spectroscopy results. Using the Bethe-Salpeter framework, we compute dielectric functions and we compare to spectra computed without excitonic effects. We find that the electron-hole interaction strongly modifies the spectra and we discuss the anisotropy of optical absorption that we find for Ga_2O_3 in relation to existing theoretical and experimental data.

I. INTRODUCTION

As suggested by their name, transparent conducting oxides (TCOs) provide the technologically desirable combination of nearly metallic conductivity with a high degree of optical transparency over the entire visible spectrum. Despite being so widespread in applications ranging from electronics[1] to sensors[2] and photovoltaics,[3,4] the fundamental properties of these materials remain quite poorly understood. In order to explore their suitability for novel applications, e.g. in the context of plasmonic materials,[5] a thorough understanding of their optical properties is necessary.

In particular, the optical properties of one of the most common TCOs, In_2O_3, have been subject to much debate due to controversy over the nature of its band gap.[6–10] Another emerging TCO, β-Ga_2O_3, also exhibits features in its absorption spectrum that remain controversial in the context of its fundamental band gap.[11–15] It was found before,[16] that for In_2O_3 some of the confusion can be traced back to the influence of free carriers (free electrons in the case of In_2O_3 and Ga_2O_3). Both In_2O_3 and Ga_2O_3 are either intrinsically n-type or intentionally doped and, hence, free-carrier concentrations in real samples can be quite large: For example, as-grown In_2O_3 typically shows 10^{19} cm^{-3} at room temperature, while Sn doping can lead to carrier concentrations in excess of 10^{21} cm^{-3}.[15,17] The maximum carrier concentrations in Ga_2O_3 have not yet reached the same levels, with the highest reported values of 10^{19} cm^{-3} observed in Si or Sn-doped samples.[15,18,19] Consequently, there are still open questions, e.g. regarding the intricate interplay of free electrons and excitonic effects. It has been shown before (e.g. for ZnO in Ref. 20) that the presence of free carriers significantly alters the optical absorption spectra as well as effective electron or hole masses.[21,22] Since these effects can be difficult to disentangle in experiment (especially if a material has a strong intrinsic n-type character), computational insight is inevitably helpful.

In this paper we aim to elucidate excitonic effects and important features of the optical absorption spectra of *ideal*, undoped In_2O_3 and Ga_3O_3 by investigating the dielectric functions of these materials over a large photon energy range. We

find that both excitonic effects due to bound states near the absorption edge and the optical anisotropy are significantly stronger in Ga_2O_3. While the former is due to a smaller dielectric screening in Ga_2O_3, the latter arises from the monoclinic crystal structure. In Section II the computational framework is summarized, while results for In_2O_3 and Ga_2O_3 are presented and discussed in Section III. Finally, Section IV summarizes the findings and concludes this paper.

II. METHODS

In order to achieve an accurate description of optical properties (including excitonic and local-field effects) from first principles, we solve the Bethe-Salpeter equation (BSE) for the optical polarization function.[23] This allows us to include two-particle (electron-hole) excitations in the description of the dielectric function. The underlying electronic structure is computed using standard density functional theory[24,25] (DFT) which yields the Kohn-Sham states that are used to compute the optical-transition matrix elements in the longitudinal approximation[26] and the statically screened Coulomb attraction as well as the unscreened exchange terms that determine the excitonic Hamiltonian. In this work, the generalized-gradient approximation for exchange and correlation as parametrized by Perdew, Burke, and Ernzerhof[27] (PBE) is used. The electron-ion interaction is described using the projector-augmented wave method[28] where we explicitly include the Ga $3d$ and In $4d$ electrons as valence states. The Vienna *Ab-initio* Simulation Package[26,29,30] and the BSE implementation discussed in Refs. 31 and 32 are used to carry out all calculations using a plane-wave basis[33] for the wave function expansions.

We use atomic geometries relaxed with the HSE06 screened hybrid functional,[34] which gives lattice parameters in better agreement to experiment for both In_2O_3 and Ga_2O_3 as compared to PBE.[35,36] Our calculated lattice constants are summarized in Table I for the 40-atom bixbyite In_2O_3 unit cell and the 10-atom monoclinic Ga_2O_3 unit cell, representing the most stable structures for each material. For the unit cell optimization and band-structure calculations we adopted an en-

	E_g^{exp} (eV)	E_g^{PBE} (eV)	Δ (eV)	$\varepsilon_{\mathrm{el.}}^0$ (ε_0)	a (Å)	b (Å)	c (Å)	β (°)
In$_2$O$_3$	2.90[10]	1.10	1.80	4.80	10.20	–	–	–
Ga$_2$O$_3$	4.86[14]	2.50	2.37	4.05	12.21	3.03	5.80	103.9

TABLE I. Lattice constants, band gaps E_g, scissor shift Δ, and static electronic dielectric constants $\varepsilon_{\mathrm{el.}}^0$ (as computed in DFT in this work) underlying the calculations of the optical absorption spectra.
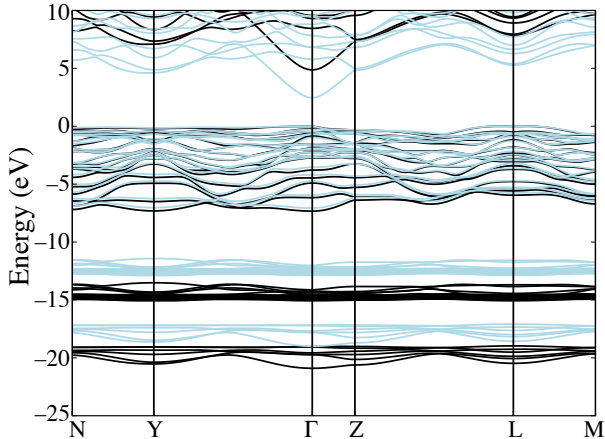
FIG. 1. Band structure of β-Ga$_2$O$_3$ as calculated with DFT-PBE (blue) and HSE (black). HSE leads to shifts of the valence and conduction bands relative to PBE, but the qualitative features of the band structure are largely reproduced.

ergy cutoff of 500 eV and integrated over the Brillouin zones with $2 \times 2 \times 2$ and $4 \times 4 \times 4$ Monkhorst-Pack **k**-point grids for In$_2$O$_3$ and β-Ga$_2$O$_3$, respectively.

Quasiparticle effects on the fundamental band gaps are approximated by using a scissor operator Δ in this work that shifts all conduction bands to higher energies by a given amount. This approach is valid for cases in which the band gap is underestimated, but the other qualitative and quantitative features of the band structure are largely reproduced by DFT-PBE compared to higher levels of theory such as HSE or the G_0W_0 approximation. This is illustrated in Fig. 1 for the band structure[37] of Ga$_2$O$_3$ calculated at the PBE and HSE levels, which shows a good agreement between the conduction band states and the upper valence band states apart from the band gap error.

One measure of the agreement is the valence-band width, which is calculated to be 7.33 eV in HSE, in close agreement with the experimental value of 7.37 eV.[14] The band width calculated in PBE is 7.07 eV, a difference of only 0.26 eV with respect to the HSE value. Considering the optical absorption onset is dominated by transitions from this upper valence band to the lowest conduction band states, the error resulting from a rigid scissor shifted is expected to be smaller than the differences arising from excitonic effects discussed in Sec. III. The agreement for In$_2$O$_3$ is similar and additionally supports that a rigid shift of the conduction bands is a valid approximation to obtaining an accurate initial electronic structure for which to calculate the optical spectrum in these materials. As shown in Fig. 1, the energies computed for Ga d states $\sim$15

eV below the VBM are underestimated by about 2 eV using PBE, however, since they are well separated from the valence-band maximum, transitions from these and lower-lying states do not contribute to the optical spectra computed in this work.

The shift Δ is the difference of the experimental band gap and the DFT-PBE one determined in our calculations for these materials: For bixbyite In$_2$O$_3$ we shift with respect to a value of 2.90 eV from coupled photoemission experiments and quasiparticle-corrected band structures.[7,9,10] For Ga$_2$O$_3$ we adopt a value of 4.86 eV as measured by angle-resolved photoemission spectroscopy (ARPES) and hybrid functional calculations.[14] The analytical model of Bechstedt et al.[38] is used to compute the screened Coulomb interaction W using the static electronic dielectric constants of 4.80 (In$_2$O$_3$) and 4.05 (Ga$_2$O$_3$) obtained on the DFT-PBE level. The band gaps and dielectric constants underlying the present work are summarized in Table I.

Since BSE calculations are computationally very challenging, we compromise between two complementary requirements for convergence: Converging the onset of the optical absorption spectrum asks for a fine sampling of the lowest single-particle transitions in the Brillouin zone (BZ), however, in order to compute optical properties over a large photon-energy range, a large number of conduction bands have to be included in the excitonic Hamiltonian. For this reason we use a more dense **k**-point grid and fewer conduction bands to compute the low-energy part of the absorption spectra close to the absorption onset. The high-energy part is computed using fewer **k** points and more conduction bands to include high-energy optical transitions. Different BSE cutoff energies (maximum non-interacting electron-hole pair energy) are employed for the different Monkhorst-Pack (MP) **k**-point grids[39] that we used, see Ref. 40 for details. Convergence is improved by displacing each grid by a small random vector to lift degeneracies that occur for unshifted MP meshes. Despite these efforts to keep the computational cost low, the resulting excitonic Hamiltonians have ranks of 360,000 and more. Even though the dielectric function is computed using a time-propagation technique[41] that scales quadratically with the rank of the excitonic Hamiltonian (which is better than the cubic scaling of direct diagonalization techniques), such computationally demanding calculations can only be carried out on high-performance super computers such as Blue Waters.

III. RESULTS AND DISCUSSION

Using this framework we computed the optical properties (dielectric functions) of ideal crystals of In$_2$O$_3$ (see Fig. 2) and Ga$_2$O$_3$ (see Fig. 3) including excitonic and local-field
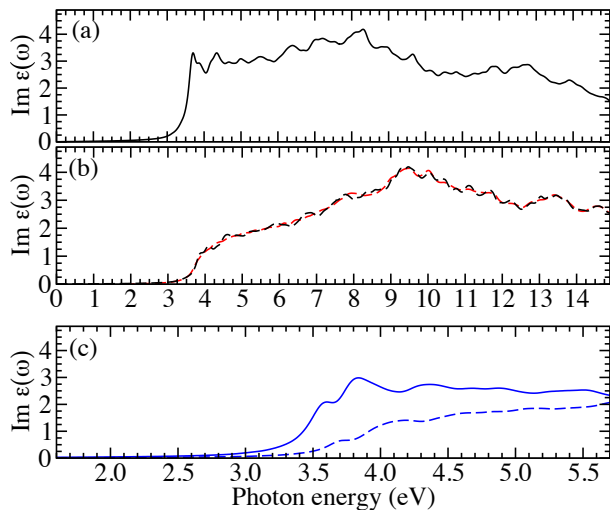
FIG. 2. Imaginary part of the dielectric function $\varepsilon(\omega)$ of cubic In$_2$O$_3$. (a) includes excitonic and local-field effects and shows the dielectric function over a large photon-energy range. In (b) we compare spectra *without* excitonic effects: The black curve is computed using the same combination of **k**-point meshes as for (a) and red is computed using a mesh of $12 \times 12 \times 12$ Monkhorst-Pack **k** points. In (c) we compare the optical absorption onset with (solid) and without (dashed) excitonic effects.

FIG. 3. Imaginary part of the (anisotropic) dielectric function $\varepsilon(\omega)$ of Ga$_2$O$_3$. Solid curves include excitonic and local-field effects, whereas dashed curves are computed without those.

effects. Due to the absence of experimentally measured dielectric functions (for instance via ellipsometry) over a large energy range, these results represent highly accurate predictions that improve on previous theoretical spectra[12,16] that neglected excitonic effects. Hence, in order to draw conclusions about the influence of excitonic effects, we included the data computed using the DFT+Δ scheme (dashed curves) in Figs. 2 and 3. Especially in the case of Ga$_2$O$_3$, the onset of optical absorption is dominated by a pronounced bound excitonic state that is visible as a large peak. For In$_2$O$_3$ the effect is less dramatic, but nevertheless a peak arising from a bound excitonic state is visible near the absorption onset [cf. Fig. 2(c)]. One reason for this peak to be smaller than the one we observe for Ga$_2$O$_3$ is the larger dielectric screening in the case of In$_2$O$_3$ (cf. Table I).

From a comparison of the DFT+Δ results with the spectra that include excitonic effects in Figs. 2 and 3, it is clear that peaks in the DFT+Δ curves experience a redshift (and, hence, are located at lower photon energies) when excitonic effects are taken into account. This general feature of peaks occurring at lower photon energies with redistributed spectral weight when excitonic effects are included is well known and was also found for other oxides[42–44] that show a similar structure of the uppermost valence and the lowest conduction band.

As previously discussed in Sec. II, the computational requirements for these calculations can limit the extent to which particular parameters such as energy cutoffs and **k**-point sampling can be improved to obtain complete convergence of the optical spectra. From Fig. 2(b) it becomes clear that the **k**-point grids used in this work to compute spectra including excitonic effects are well converged at least on a single-particle
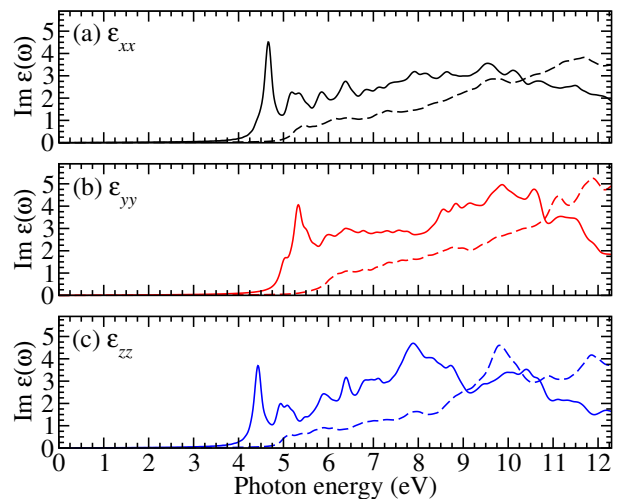
DFT-PBE level, as the difference between the two curves in Fig. 2(b) is very small. However, we note that it is computationally challenging to reproduce a plateau structure like the one found on DFT-PBE level between 5 and 8 eV in Fig. 2(b) also in the BSE approach [Fig. 2(a)] due to the extremely high computational cost. A similar effect is visible for the bound excitonic state in In$_2$O$_3$: improving the **k**-point sampling going from Fig. 2(a) to Fig. 2(c) improves the fine structure of our results. Nevertheless, except for the fine structure of the curves, the overall shape of our computed curves is well converged. We also note that with increasing photon energies the influence of the DFT+Δ approximation becomes more severe, typically leading to peaks in the theoretical spectra occurring at too low energies (by about $0.5 - 1$ eV).[44]

For In$_2$O$_3$ we do not observe any optical anisotropy since the material is cubic. As seen in Fig. 3, this is dramatically different for monoclinic Ga$_2$O$_3$, which shows a pronounced optical anisotropy across the entire range of photon energies. The anisotropy of the Ga$_2$O$_3$ absorption edge has been reported on extensively, where experimental transmission measurements indicate the lowest onset at $\sim 4.6 - 4.7$ eV for light polarized parallel to the crystallographic c axis ($E \parallel c$) and higher by ~ 0.3 eV for light polarized parallel to the b axis ($E \parallel b$).[45–48] This has previously been explained by Yamaguchi in the context of direct symmetry-allowed and -forbidden transitions between the uppermost valence bands at Γ and the conduction band minimum of Ga s character.[12] Their analysis of the irreducible representations of the valence band states at the Γ point in the calculated band structure suggest that the $E \parallel b$ absorption onset should be 0.67 eV higher than that of the absorption $E \parallel c$. This difference qualitatively describes the anisotropy observed, but is larger than the experimental offset of ~ 0.3 eV.[12,45–48]

Similar to the results obtained by Yamaguchi,[12] we observe the lowest onset for ε_{zz}, which occurs only slightly below the one for ε_{xx} by $0.2 - 0.3$ eV. From the spectra of ε_{yy} in Fig. 3(b),

it is seen that the onset for absorption of light polarized parallel to the b axis starts at significantly higher photon energies than for light polarized along the other crystallographic axes. This is consistent with the observation of a rapid decrease in the transmission spectra of Ga_2O_3 for light polarized perpendicular to the b axis ($E \perp b$) over the range of $4.4 - 4.6$ eV.[46,48] Furthermore, this optical anisotropy is also seen for other peak structures at higher photon energies that either occur only for ε_{zz} (e.g. around 8 eV) or ε_{yy} (e.g. around 10 eV). Considering our spectra without excitonic effects in Fig. 3, we observe a similar shift as Yamaguchi of the spectra between the onsets of the ε_{zz}, ε_{xx}, and ε_{yy} dielectric functions, and reproduce the qualitative and quantitative features.[12] However with excitonic effects, the peaks shift substantially, with the ε_{zz} edge decreasing by ~ 0.5 eV as compared to the DFT+Δ results (Fig. 3c) and similarly large shifts for the other polarizations.

Both the intensities and the relative shifts of the excitonic peaks are sensitive to a number of factors, one of which is the choice of the ε_{el}^0 used to screen the electron-hole interaction. The value used (see Table I) is calculated at the PBE level and excludes any contributions due to ionic screening. This approximation may be insufficient for materials which exhibit a strong electron-phonon coupling, which may be a concern in Ga_2O_3 as holes have been reported to immediately self-trap, forming small polarons.[49,50] Therefore, a higher effective dielectric constant that is between the electronic (3.61) and static (10.2) values[51] may be necessary to obtain more accurately resolved optical spectra, particularly in the proximity of the absorption edge. Considering this and the strong excitonic features, the optical spectra of Ga_2O_3 require further study both theoretically and experimentally.

IV. CONCLUSIONS

In this work we used modern theoretical-spectroscopy techniques based on the solution of the Bethe-Salpeter equation for the optical-polarization function to compute the optical absorption properties of cubic In_2O_3 and monoclinic Ga_2O_3. This allows us to take excitonic and local-field effects into account when computing the dielectric function of these two materials. While the large unit cells of these oxides (in particular of In_2O_3) render these calculations computationally very challenging, we do find a satisfactory convergence across a large photon energy range. We find that excitonic effects play an important role for the optical-absorption properties of both materials, but in particular for Ga_2O_3 for which we find a strong bound excitonic state at the absorption edge and a remarkably strong optical anisotropy. Despite these strong excitonic features, the optical gap of β-Ga_2O_3 remains significantly larger than those of other TCOs and suggests it is well-suited for applications such as solar-blind photodiodes that exploit its transparency in the UV.[52,53] From comparison to experiment and other calculations (that neglect excitonic effects), we find indications that the strong electron-phonon coupling in Ga_2O_3 significantly affects the dielectric screening. These effects deserve further attention in future experimental and theoretical studies to fully resolve the optical spectra of this emerging TCO.

* varley2@llnl.gov
† schleife@illinois.edu

[1] A. P. Ramirez, Science **315**, 1377 (2007).

[2] H. E. Endres, W. Göttler, R. Hartinger, S. Drost, W. Hellmich, G. Müller, C. B. v. Braunmühl, A. Krenkow, C. Perego, and G. Sberveglieri, Sensor. Actuat. B-Chem. **36**, 353 (1996).

[3] E. Fortunato, D. Ginley, H. Hosono, and D. C. Paine, MRS Bull. **32**, 242 (2007).

[4] C.-H. M. Chuang, P. R. Brown, V. Bulović, and M. G. Bawendi, Nat. Mater. (2014), 10.1038/nmat3984.

[5] A. Boltasseva, MRS Bull. **39**, 461 (2014).

[6] A. Walsh, J. L. F. Da Silva, S.-H. Wei, C. Körber, A. Klein, L. Piper, A. DeMasi, K. Smith, G. Panaccione, P. Torelli, D. Payne, A. Bourlange, and R. G. Egdell, Phys. Rev. Lett. **100**, 167402 (2008).

[7] L. F. J. Piper, A. DeMasi, S. W. Cho, K. E. Smith, F. Fuchs, F. Bechstedt, C. Körber, A. Klein, D. J. Payne, and R. G. Egdell, Appl. Phys. Lett. **94**, 022105 (2009).

[8] N. Novkovski and A. Tanuševski, Semicond. Sci. Technol. **23**, 095012 (2008).

[9] V. Scherer, C. Janowitz, A. Krapf, H. Dwelk, D. Braun, and R. Manzke, Appl. Phys. Lett. **100**, 212108 (2012).

[10] K. Irmscher, M. Naumann, M. Pietsch, Z. Galazka, R. Uecker, T. Schulz, R. Schewski, M. Albrecht, and R. Fornari, Phys. Status Solidi A **211**, 54 (2013).

[11] T. Matsumoto, M. Aoki, A. Kinoshitaï, and T. Aono, Jpn. J. Appl. Phys. **13** (1974).

[12] K. Yamaguchi, Solid State Commun. **131**, 739 (2004).

[13] K. Shimamura, E. G. Víllora, T. Ujiie, and K. Aoki, Appl. Phys. Lett. **92**, 201914 (2008).

[14] M. Mohamed, C. Janowitz, I. Unger, R. Manzke, Z. Galazka, R. Uecker, R. Fornari, J. R. Weber, J. B. Varley, and C. G. Van de Walle, Appl. Phys. Lett. **97**, 211903 (2010).

[15] C. Janowitz, V. Scherer, M. Mohamed, A. Krapf, H. Dwelk, R. Manzke, Z. Galazka, R. Uecker, K. Irmscher, R. Fornari, M. Michling, D. Schmeißer, J. R. Weber, J. B. Varley, and C. G. Van de Walle, New J. Phys. **13**, 085014 (2011).

16 F. Fuchs and F. Bechstedt, Phys. Rev. B **77**, 155107 (2008).

17 N. Preissler, O. Bierwagen, A. T. Ramu, and J. S. Speck, Phys. Rev. B **88**, 085305 (2013).

18 E. G. Víllora, K. Shimamura, Y. Yoshikawa, T. Ujiie, and K. Aoki, Appl. Phys. Lett. **92**, 202120 (2008).

19 K. Sasaki, M. Higashiwaki, and A. Kuramata, Appl. Phys. Express **6**, 086502 (2013).

20 A. Schleife, C. Rödl, F. Fuchs, K. Hannewald, and F. Bechstedt, Phys. Rev. Lett. **107**, 236405 (2011).

21 S. K. V. Farahani, C. F. McConville, T. D. Veal, and A. Schleife, Proc. SPIE **8626**, 862604 (2013).

22 C. Rödl and A. Schleife, Phys. Status Solidi A **211**, 74 (2014).

23 G. Onida, L. Reining, and A. Rubio, Rev. Mod. Phys. **74**, 601 (2002).

24 P. Hohenberg and W. Kohn, Phys. Rev. **136**, B864 (1964).

25 W. Kohn and L. J. Sham, Phys. Rev. **140**, A1133 (1965).

26 M. Gajdoš, K. Hummer, G. Kresse, J. Furthmüller, and F. Bechstedt, Phys. Rev. B **73**, 045112 (2006).

27 J. P. Perdew, K. Burke, and M. Ernzerhof, Phys. Rev. Lett. **77**, 3865 (1996).

28 P. E. Blöchl, Phys. Rev. B **50**, 17953 (1994).

29 G. Kresse and D. Joubert, Phys. Rev. B **59**, 1758 (1999).

30 G. Kresse and J. Furthmüller, Phys. Rev. B **54**, 11169 (1996).

31 C. Rödl, F. Fuchs, J. Furthmüller, and F. Bechstedt, Phys. Rev. B **77**, 184408 (2008).

32 F. Fuchs, C. Rödl, A. Schleife, and F. Bechstedt, Phys. Rev. B **78**, 085103 (2008).

33 Cutoff energies of the plane-wave basis were slightly reduced to 400 eV for the Bethe-Salpeter calculations for both In_2O_3 and Ga_2O_3.

34 J. Heyd, G. E. Scuseria, and M. Ernzerhof, J. Chem. Phys. **124**, 219906 (2006).

35 J. B. Varley, J. R. Weber, A. Janotti, and C. G. Van de Walle, Appl. Phys. Lett. **97**, 142106 (2010).

36 J. B. Varley, H. Peelaers, A. Janotti, and C. G. Van de Walle, J. Phys.: Condens. Matter **23**, 334212 (2011).

37 S. Curtarolo, W. Setyawan, G. L. Hart, M. Jahnatek, R. V. Chepulskii, R. H. Taylor, S. Wang, J. Xue, K. Yang, O. Levy, M. J. Mehl, H. T. Stokes, D. O. Demchenko, and D. Morgan, Comput. Mater. Sci. **58**, 218 (2012).

38 F. Bechstedt, R. D. Sole, G. Cappellini, and L. Reining, Solid State Commun. **84**, 765 (1992).

39 H. J. Monkhorst and J. D. Pack, Phys. Rev. B **13**, 5188 (1976).

40 In the case of In_2O_3, $5 \times 5 \times 5$ MP **k** points and 12.5 eV for the BSE cutoff were used for photon energies below 7.67 eV and $4 \times 4 \times 4$ / 17 eV for higher photon energies. In addition, $6 \times 6 \times 6$ MP **k** points and 7.0 eV BSE cutoff were used to resolve the absorption onset of In_2O_3 in Fig. 2(c). For Ga_2O_3 we used $12 \times 12 \times 12$ MP **k** points and 12.5 eV for the BSE cutoff.

41 W. G. Schmidt, S. Glutsch, P. H. Hahn, and F. Bechstedt, Phys. Rev. B **67**, 085307 (2003).

42 A. Schleife, J. B. Varley, F. Fuchs, C. Rödl, F. Bechstedt, P. Rinke, A. Janotti, and C. G. Van de Walle, Phys. Rev. B **83**, 035116 (2011).

43 A. Schleife, C. Rödl, F. Fuchs, J. Furthmüller, and F. Bechstedt, Phys. Rev. B **80**, 035112 (2009).

44 A. Schleife and F. Bechstedt, J. Mater. Res. **27**, 2180 (2012), Focus Issue: Oxide Semiconductors.

45 H. H. Tippins, Phys. Rev. **140**, A316 (1965).

46 N. Ueda, H. Hosono, R. Waseda, and H. Kawazoe, Appl. Phys. Lett. **70**, 3561 (1997).

47 E. G. Víllora, M. Yamaga, T. Inoue, S. Yabasi, Y. Masui, T. Sugawara, and T. Fukuda, Jpn. J. Appl. Phys. **41**, L622 (2002).

48 T. Onuma, S. Fujioka, T. Yamaguchi, M. Higashiwaki, K. Sasaki, T. Masui, and T. Honda, Appl. Phys. Lett. **103**, 041910 (2013).

49 T. Harwig, G. J. Wubs, and G. J. Dirksen, Solid State Commun. **18**, 1223 (1976).

50 J. B. Varley, A. Janotti, C. Franchini, and C. G. Van de Walle, Phys. Rev. B **85**, 081109 (2012).

51 M. Passlack, N. Hunt, E. F. Schubert, G. J. Zydzik, M. Hong, J. P. Mannaerts, R. L. Opila, and R. J. Fischer, Appl. Phys. Lett. **64**, 2715 (1994).

52 T. Oshima, T. Okuno, N. Arai, N. Suzuki, S. Ohira, and S. Fujita, Appl. Phys. Express **1**, 011202 (2008).

53 S. Nakagomi, T. Momo, S. Takahashi, and Y. Kokubun, Appl. Phys. Lett. **103**, 072105 (2013).